Power Flow Calculation for VSC-based AC/DC Hybrid Systems Based on Fast and Flexible Holomorphic Embedding

Peichuan Tian, *Student Member*, *IEEE*, Yexuan Jin, Ning Xie, Chengmin Wang, and Chunyi Huang, *Member*, *IEEE*

***Abstract*—The power flow (PF) calculation for AC/DC hybrid systems based on voltage source converter (VSC) plays a crucial role in the operational analysis of the new energy system. The fast and flexible holomorphic embedding (FFHE) PF method, with its non-iterative format founded on complex analysis theory, exhibits superior numerical performance compared with traditional iterative methods. This paper aims to extend the FFHE method to the PF problem in the VSC-based AC/DC hybrid system. To form the AC/DC FFHE PF method, an AC/DC FFHE model with its solution scheme and a sequential AC/DC PF calculation framework are proposed. The AC/DC FFHE model is established with a more flexible form to incorporate multiple control strategies of VSC while preserving the constructive and deterministic properties of original FFHE to reliably obtain operable AC/DC solutions from various initializations. A solution scheme for the proposed model is provided with specific recursive solution processes and accelerated Padé approximant. To achieve the overall convergence of AC/DC PF, the AC/DC FFHE model is integrated into the sequential calculation framework with well-designed data exchange and control mode switching mechanisms. The proposed method demonstrates significant efficiency improvements, especially in handling scenarios involving control mode switching and multiple recalculations. In numerical tests, the superiority of the proposed method is confirmed through comparisons of accuracy and efficiency with existing methods, as well as the impact analyses of different initializations.**

***Index Terms*—AC/DC power flow, holomorphic embedding, numerical performance, voltage source converter (VSC).**

I. Introduction

THE AC/DC hybrid systems based on voltage source converter (VSC) possess significant advantages in achieving flexible control, high-capacity transmission, and integration of renewable energy sources such as photovoltaic (PV) and wind power [1]-[3]. Power flow (PF) calculation in AC/DC hybrid system serves as the basic analytical tool for hybrid system planning, operation analysis, and stability assessments. Considering the complexity of hybrid topologies and the diversity in control modes of VSCs, the development of PF methods for rapidly, accurately, and reliably obtaining accurate AC/DC PF solutions has been a focal research point.

Current AC/DC PF methodologies can be categorized into unified [4]-[7] and sequential [8]-[11] methods. The unified method formulates a high-dimensional nonlinear equation by integrating AC and DC subsystems with converter equations, leading to rapid convergence. However, computational efficiency may be diminished in solving large systems. In contrast, the sequential method, offering superior scalability and flexibility, solves subsystem and converter equations independently, yet faces challenges in ensuring overall algorithm convergence due to data exchange between modules.

Using iterative techniques such as the Newton-Raphson (N-R) method to solve the nonlinear PF equations constitutes the central procedure in both unified [5] and sequential [8] methods. In most AC cases, N-R-based PF method converges to the feasible solution particularly. However, the AC/DC PF methods based on N-R method encounter several challenges:

1) The most notable drawback of the N-R-based PF method is that its convergence is highly sensitive to a reasonable initial guess. If the initial guess deviates significantly from the true PF solution, the method may fail to converge, leading to computational failure [12], [13].

2) To solve the AC/DC PF equations by N-R method, the Jacobian matrix must incorporate multiple control variables of the VSC [9]. This leads to extra modifications and recalculations when switching converter control strategies, thereby escalating computational complexity. Moreover, varying control parameters increase the risk of the Jacobian matrix becoming singular, ultimately resulting in solution failure.

3) The high-dimensional and nonlinear nature yields multiple solutions of PF equation. Only the high-voltage (HV) solution is operable for the system [14]. In the application of N-R-based PF method, convergence to HV solution cannot

Manuscript received: February 21, 2024; revised: April 8, 2024; accepted: May 22, 2024. Date of CrossCheck: May 22, 2024. Date of online publication: July 5, 2024.

P. Tian, N. Xie, C. Wang (corresponding author), and C. Huang are with Key Laboratory of Control of Power Transmission and Conversion (Ministry of Education), Shanghai Jiao Tong University, Shanghai 200240, China (e-mail: desmondtian@sjtu.edu.cn; ningxie@sjtu.edu.cn; wangchengmin@sjtu.edu.cn; h_chunyi@sjtu.edu.cn).

Y. Jin is with the State Grid Hangzhou Power Supply Company, Hangzhou 310009, China (e-mail: 260737385@qq.com).

DOI: 10.35833/MPCE.2024.000185

be guaranteed due to the unpredictable convergence property of these methods.

To address the aforementioned issues, a non-iterative PF method based on holomorphic embedding (HE) is firstly proposed in [15]. The HE PF method, which is based on complex analysis, transforms PF equations into those that satisfy Cauchy-Riemann conditions by embedding complex variables, and obtains solutions through analytic continuation techniques. Later in [16] and [17], by refining the structure of the embedded PF equation, the HE PE method is extended to be applicable to general AC PF problems with PV buses and nonlinear DC PF problems. Benefiting from the non-iterative solving process, the HE PF method provides a theoretical guarantee of converging to HV solutions as long as they exist [18]. It enables the HE PF method to exhibit superior numerical performance compared with the N-R-based method. The implementation of the HE method has been extended to encompass modeling of flexible AC transmission system (FACTS) devices [19], [20], analysis of voltage stability [21], [22], and identification of vulnerable buses [23] in AC power systems, showcasing its robust versatility and scalability.

HE based AC/DC PF method is investigated in [24], [25], preserving the advantageous feature of reliable convergence to HV solutions. The extension of such method to the AC/DC microgrid is investigated in [26] - [28]. HE models of power electronic devices, distributed generations, and impedance, current, and power (ZIP) loads are developed in these studies while various operating scenarios of AC/DC microgrid are considered. However, there are still two main unresolved challenges in the HE based AC/DC PF based AC/DC PF method. First of all, the HE based AC/DC PF method requires the generation of more complex coefficient matrices that consider variables of AC and DC subsystems, as well as converter stations. This complexity results in the HE based AC/DC PF method not exhibiting superior numerical performance in terms of computational speed. In fact, its computational speed can be much slower than the N-R-based method [8]. More importantly, HE method in [15] and [16] suffers from one major limitation: a fixed initialization, usually the zero injection state (flat start) of the embedded system, is required for each HE PF calculation. Meanwhile, due to the restriction of VSC power limit, the VSC control mode switching becomes necessary during the AC/DC PF calculation. Each switch between control modes inevitably triggers the recalculation of AC/DC PF. Existing HE based AC/DC PF methods only allow the initialization to be reset to the flat start after each control mode switching, instead of taking the latest solved PF solution as a new start. Such recalculations will significantly diminish the efficiency of the AC/DC PF method.

The fast and flexible holomorphic embedding (FFHE) method, as proposed in [29] - [31], introduces a flexible embedding form that accommodates various state vectors as initial guesses. Additionally, it demonstrates faster convergence and superior computational efficiency compared with the original HE methods when dealing with AC PF problem. Consequently, the FFHE method appears to offer a promising solution to the previously mentioned challenges in the AC/DC PF calculation.

To Introduce the FFHE method into the AC/DC PF calculation, several key issues still need to be addressed:

1) In [29], it only provides the FFHE model for the pure AC systems, which cannot be simply and directly applied to AC/DC hybrid system. At the same time, there are various manners of embedding technique, but not all of them are suitable. Thus, the challenging task of properly constructing the FFHE models for the AC/DC PF problem remains. Here, "properly" implies that the newly proposed model should not only retain the constructive and deterministic properties of the original FFHE model but also be tailored to solve the variables of the DC subsystem associated with VSC stations in multiple control modes simultaneously.

2) The calculation of converter losses and the control mode switching require well-designed AC/DC sequential calculation framework to achieve the overall convergence of AC/DC FFHE results under the constraints of VSC stations.

3) Moreover, the effect of the FFHE method on computational accuracy and convergence still needs further testing and explanation when applied to the AC/DC PF calculation.

Inspired by the FFHE method, a novel PF calculation method based on FFHE for VSC-based AC/DC hybrid systems is proposed in this paper. The primary contributions of this study are outlined as follows:

1) By considering the detailed model of VSC stations, we construct the PF model of the AC/DC hybrid system, upon which the AC/DC FFHE model is developed. The proposed model not only possesses a more flexible form to incorporate multiple control strategies of VSC, but also preserves the constructive and deterministic properties that allow it to obtain operable AC/DC PF solutions from various initializations.

2) A solution scheme for the AC/DC FFHE model is designed, including the construction of recursive solution for AC/DC FFHE model and the use of accelerated Padé approximant to determine power series coefficients and the numerical results of AC/DC PF solutions.

3) A sequential framework for AC/DC PF calculation is introduced, integrating the FFHE solution scheme, data exchange mechanism between AC and DC subsystems, as well as VSC limit check and control mode switching mechanism. While achieving the overall AC/DC PF convergence, this framework facilitates the use of the intermediate PF results as the default start for each recalculation, leading to a noteworthy reduction in overall runtime.

The remainder of this paper is organized as follows. In Section II, the analysis of the steady-state model of the VSC-based AC/DC hybrid system is presented. Building upon this steady-state model, the AC/DC FFHE model is established in Section III. Section IV introduces the sequential computation framework to form the AC/DC FFHE PF method. By comparing with existing methods, the computational performance of the proposed method is demonstrated through multiple numerical tests in Section V. Finally, Section VI draws conclusions.

II. Steady-state Model of VSC-based AC/DC Hybrid Systems

The schematic representation in Fig. 1 illustrates the topology of the VSC-based AC/DC hybrid system. It consists of AC subsystem, DC subsystem, and converter station. The steady-state PF models of these three parts are particularized in this section.

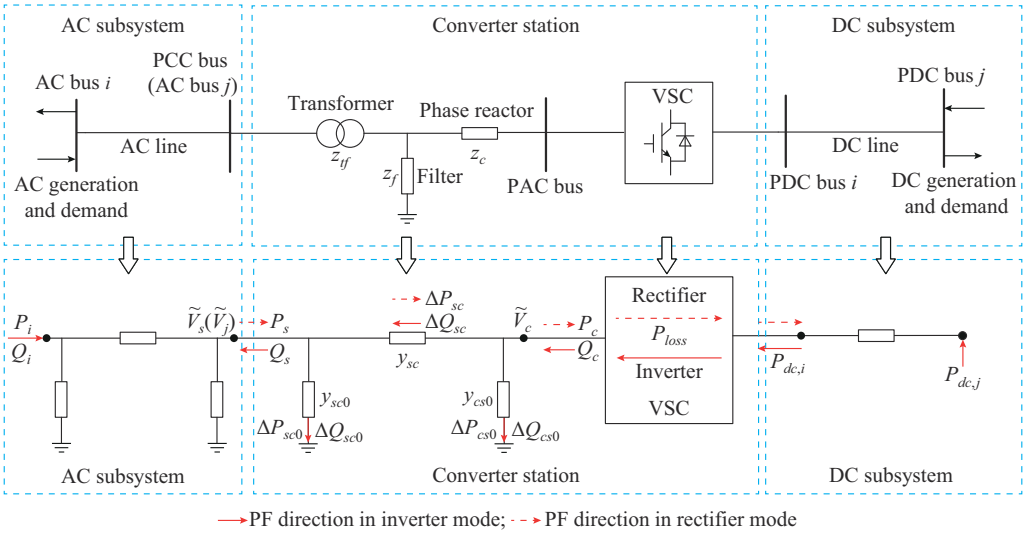

Fig. 1. Topology of VSC-based AC/DC hybrid system.

A. VSC Station

The VSC station is modeled by assuming a separate branch comprising a transformer, a phase reactor, and a low-pass filter [8]. The connections of the VSC station to the AC and DC subsystems are established through the points of common coupling (PCC bus) and points of DC connection (PDC bus), respectively. The interconnection between the converter and the station is referred to as the points of AC connection (PAC bus). By applying the Y-Δ transformation, the π equivalent circuit of the converter station is obtained, as shown in Fig. 1, in which the series and shunt parameters y_{sc}, y_{sc0}, and y_{cs0} can be determined by z_c, z_{tf}, and z_f, which denote the complex impedances of phase reactor, transformer, and filter, respectively.

Define $\tilde{V}_s$ and $\tilde{V}_c$ as the nodal voltages of PCC bus and PAC bus, respectively. $\tilde{S}_s = P_s + \mathrm{j}Q_s$ denotes the power exchange between the AC system and PCC bus. $\tilde{S}_c = P_c + \mathrm{j}Q_c$ denotes the power exchange between the VSC and the PAC bus. $\Delta\tilde{S}_{sc} = \Delta P_{sc} + \mathrm{j}\Delta Q_{sc}$ denotes the series branch power losses. $\Delta\tilde{S}_{sc0} = \Delta P_{sc0} + \mathrm{j}\Delta Q_{sc0}$ and $\Delta\tilde{S}_{cs0} = \Delta P_{cs0} + \mathrm{j}\Delta Q_{cs0}$ denote the shunt branch power injections. Then, the power balance equation inside the converter station, e. g., inverter mode shown in Fig. 1, is given as:

$$\tilde{S}_c = \tilde{S}_s + \Delta\tilde{S}_{sc} + \Delta\tilde{S}_{sc0} + \Delta\tilde{S}_{cs0} \tag{1}$$

In (1), with known $\tilde{S}_s$, $\Delta\tilde{S}_{sc0}$ can be determined by (2a). The symbol * represents the conjugation. Meanwhile, the nodal voltage $\tilde{V}_c$ can be obtained via (3). Then, $\Delta\tilde{S}_{cs0}$ and $\Delta\tilde{S}_{sc}$ can be computed by (2b) and (2c), respectively.

$$\Delta\tilde{S}_{sc0} = \left|\tilde{V}_s\right|^2 y_{sc0}^* \tag{2a}$$

$$\Delta\tilde{S}_{cs0} = \left|\tilde{V}_c\right|^2 y_{cs0}^* \tag{2b}$$

$$\Delta\tilde{S}_{sc} = \left|\left(\tilde{S}_s + \Delta\tilde{S}_{sc0}\right)\Big/\tilde{V}_s\right|^2 \times 1/y_{sc} \tag{2c}$$

$$\tilde{V}_c = \tilde{V}_s + \left(\tilde{S}_s + \Delta\tilde{S}_{sc0}\right)^*\Big/\left(\tilde{V}_s^* y_{sc}\right) \tag{3}$$

Considering the active power loss of the VSC, the active power exchange between PAC and PDC buses is modeled as:

$$P_{dc} = -P_c - P_{loss} \tag{4}$$

The converter losses P_{loss} are quadratically dependent on the converter current $\tilde{I}_c$ [8], [10], as shown in (5), where a, b, and c are the constants related to the types of VSC.

$$P_{loss} = a + b\left|\tilde{I}_c\right| + c\left|\tilde{I}_c\right|^2 \tag{5}$$

The converter current magnitude can be obtained by:

$$I_c = \sqrt{P_c^2 + Q_c^2}\Big/\left|\tilde{V}_c\right| \tag{6}$$

B. Types of VSC Station Buses

The VSC station can independently control the active and reactive power outputs through multiple combinations of *d*-*q*-axis control modes [5], [9]. The *d*-axis control mode set comprises P_s-control, V_{dc}-control, and droop control, while the *q*-axis control mode set encompasses Q_s-control and V_s-control. V_{dc} is the DC voltage at PDC bus; and V_s is the AC voltage magnitude at PCC bus. Different control strategies directly influence the PF characteristics of PCC bus and PDC bus within the converter station. The bus type classification according to various control strategies is summarized as follows.

As shown in Table I, the PCC bus mainly behaves as the *PQ* bus or *PV* bus, which is the same as the pure AC bus. The PDC bus can be categorized into several types based on different implemented control modes, including:

1) Constant-V_{dc} bus under V_{dc}-control: the DC voltage at

PDC bus maintains while the active power injection varies. Due to its similarity to the AC slack bus, this type of PDC bus is typically treated as the slack bus for the DC system.

2) Constant-P_{dc} bus under P_s-control: the active power injection at PDC bus stays constant while the DC bus voltage needs further determination.

3) Voltage droop bus: the active power varies with voltage changes to a predetermined droop constant K_i, reference voltage $V_{ref,i}$, and reference active power $P_{ref,i}$ via control equation (7), thereby achieving flexible power distribution among DC buses. Note that constant-P_{dc} bus can be treated as a special droop bus with $K_i=0$.

$$K_i\left(V_{dc,i}-V_{ref,i}\right)=P_{ref,i}-P_{dc,i} \tag{7}$$

where $V_{dc,i}$ is the DC voltage at PDC bus i; and $P_{dc,i}$ is the DC active power injection at PDC bus i.

TABLE I
CONTROL MODES AND BUS TYPES

d-axis control	q-axis control	PCC bus type	PDC bus type
P_s-control	Q_s-control	PQ	Constant-P_{dc}
P_s-control	V_s-control	PV	Constant-P_{dc}
V_{dc}-control	Q_s-control	PQ	Constant-V_{dc}
V_{dc}-control	V_s-control	PV	Constant-V_{dc}
Droop	Q_s-control	PQ	Droop
Droop	V_s-control	PV	Droop

C. AC and DC Subsystems

Consider an AC/DC hybrid system with an N-bus AC system and an M-bus DC system interlinked via VSC stations. Note that PCC buses are considered as the decoupling boundary between the AC subsystem and the VSC station. Therefore, an AC subsystem comprises all pure AC buses and PCC buses.

The power balance equation for the pure AC bus or PCC bus, specifically operating as a PQ bus i, is given by (8).

$$\tilde{V}_i^*\sum_{k=1}^{N}Y_{ik}\tilde{V}_k=\tilde{S}_i^* \tag{8}$$

where $\tilde{V}_i$ is the AC voltage at bus i; $\tilde{V}_k$ is the AC voltage at bus k; Y_{ik} is the element of admittance matrix; and $\tilde{S}_i=P_i+\mathrm{j}Q_i$ is the apparent power at AC bus i, $P_i=P_{Gi}-P_{Di}$ and $Q_i=Q_{Gi}-Q_{Di}$ are the active and reactive power injections determined by generation power P_{Gi}, Q_{Gi} and demand power P_{Di}, Q_{Di} at AC bus i.

Specifically, for the PV bus i in the AC system, its PF characteristic can be described by (9).

$$\mathrm{Re}\left\{\tilde{V}_i^*\sum_{k=1}^{N}Y_{ik}\tilde{V}_k\right\}=P_i \tag{9a}$$

$$\left|\tilde{V}_i\right|=V_{sp,i} \tag{9b}$$

where $V_{sp,i}$ is the pre-specified voltage magnitude for bus i; and $\mathrm{Re}\{\cdot\}$ represents the real part of a complex phasor.

For PAC bus, with the AC voltage $\tilde{V}_s$ and power injection $\tilde{S}_s$ at PCC bus known by solving AC subsystem PF, $\tilde{V}_c$ and $\tilde{S}_c$ at the converter side can be calculated by (1)-(3). Then, converter losses can be determined by (5) and (6) so that the power balance between PDC and PAC buses can be established according to (4).

The DC subsystem contains all PDC buses. For PDC bus i, the PF equation is derived as:

$$pV_{dc,i}\sum_{k=1}^{M}G_{ik}V_{dc,k}=P_{dc,i} \tag{10}$$

where $p=1$ or 2 for a monopolar or bipolar DC configuration; and G_{ik} is the conductance component of Y_{ik} in the admittance matrix. When multiple control modes in Section II-B are considered, (10) is rewritten as (11) by substituting (7) into (10) for the bus i under constant-P_{dc} and droop control:

$$pV_{dc,i}\sum_{k=1}^{M}G_{ik}V_{dc,k}=K_i\left(V_{ref,i}-V_{dc,i}\right)+P_{ref,i} \tag{11}$$

For PDC bus i under constant-V_{dc}, (12) is satisfied.

$$V_{dc,i}=V_{spdc,i} \tag{12}$$

where $V_{spdc,i}$ is the pre-specified DC voltage for PDC bus i .

III. AC/DC FFHE MODEL

The primary procedure of FFHE involves the following steps: ① establishing embedded PF models for PF equations; ② representing the HE function of nodal voltage by power series and determining corresponding coefficients; and ③ computing the summation of the power series to ascertain the PF solution at the target state.

A. FFHE Model for AC Subsystem

Since the PCC buses, as analyzed in Section II, generally behave as PQ or PV buses, the AC FFHE model in [29] can be applied to PCC buses together with pure AC buses. By introducing a complex variable $\alpha\in\mathbb{C}$ into AC PF equations (8) and (9), the AC FFHE model is formulated as:

$$\tilde{V}_i^*\left(\alpha^*\right)\sum_{k=1}^{N}Y_{ik}\tilde{V}_k(\alpha)=v_i^*\sum_{k=1}^{N}Y_{ik}v_k+\alpha\left(\tilde{S}_i^*-v_i^*\sum_{k=1}^{N}Y_{ik}v_k\right) \tag{13}$$

$$\begin{aligned}&\tilde{V}_i^*\left(\alpha^*\right)\sum_{k=1}^{N}Y_{ik}\tilde{V}_k(\alpha)+\tilde{V}_i(\alpha)\sum_{k=1}^{N}Y_{ik}^*\tilde{V}_k^*\left(\alpha^*\right)=\\&\quad v_i^*\sum_{k=1}^{N}Y_{ik}v_k+v_i\sum_{k=1}^{N}Y_{ik}^*v_k^*+\\&\quad\alpha\left[2P_i-\left(v_i^*\sum_{k=1}^{N}Y_{ik}v_k+v_i\sum_{k=1}^{N}Y_{ik}^*v_k^*\right)\right]\end{aligned} \tag{14a}$$

$$\tilde{V}_i(\alpha)\tilde{V}_i^*\left(\alpha^*\right)=v_iv_i^*+\alpha\left(V_{sp,i}^2-v_iv_i^*\right) \tag{14b}$$

where $v_i\in\mathbb{C}/\{0\}$ is a predefined adjustable constant, which denotes the initial value of $\tilde{V}_i(\alpha)$ by $\tilde{V}_i(0)=v_i$ at the reference state of $\alpha=0$. At the target state $\alpha=1$, the original PF equations (8) and (9) are recovered from (13) and (14), and $\tilde{V}_i(1)$ denotes the target nodal voltage solution. Specially for the slack AC bus i, $\tilde{V}_i(0)=v_i$ and $\tilde{V}_i(1)=\tilde{V}_{sp,i}$ are satisfied. $\tilde{V}_{sp,i}$ is the pre-specified slack AC bus voltage phasor.

The HE function of AC nodal voltage $\tilde{V}_i(\alpha)$ and its conjugate $\tilde{V}_i^*\left(\alpha^*\right)$ are expressed by power series expansions cen-

tered at 0 as:

$$\tilde{V}(\alpha)=\sum_{q=0}^{\infty}u_{iq}\alpha^{q} \tag{15a}$$

$$\tilde{V}_i^{*}(\alpha^{*})=\sum_{q=0}^{\infty}u_{iq}^{*}\alpha^{q} \tag{15b}$$

where u_{iq} is the coefficient of the q^{th} term in the power series.

B. FFHE Model for DC Subsystem

Due to different PF characteristics between AC buses and VSC controlled DC buses, the original FFHE model in [29] cannot be directly used for DC subsystem. To be adapted to various VSC control modes while upholding the superior properties of original FFHE model, the newly proposed DC FFHE model should meet the following three conditions.

1) At the initial state 0, the model has a known solution. The solution should be adjustable to provide a flexible start for FFHE.

2) At the target state 1, the original PF equation (11) should be recovered.

3) The model should incorporate multiple control variables to generally represent all kinds of VSC controlled buses. It should also be able to adapt to changes in corresponding control variables with convenient operations while maintaining the model structure.

Note that unlike the AC FFHE model, all variables involved in the DC FFHE model are real numbers instead of complex ones. However, it is crucial that the embedding parameter remains complex. This is because, as stipulated by Stahl's theorem [32], [33], working in the complex plane ensures the convergence and effectiveness of the analytic continuation procedure employed in the numerical summation of the power series. The proposed DC FFHE model is then formulated as follows.

Equation (16a) presents the DC FFHE model of PF balance equation (11) for constant-P_{dc} and droop buses, while (16b) represents the model for constant-V_{dc}.

$$V_{dc,i}(\alpha)\left(p\sum_{k=1}^{M}G_{ik}V_{dc,k}(\alpha)+K_i\right)=v_{dc,i}\left(p\sum_{k=1}^{M}G_{ik}v_{dc,k}+K_i\right)+\alpha\left[\left(K_iV_{ref,i}+P_{ref,i}\right)-v_{dc,i}\left(p\sum_{k=1}^{M}G_{ik}v_{dc,k}+K_i\right)\right] \tag{16a}$$

$$V_{dc,i}=v_{dc,i}+\alpha\left(V_{spdc,i}-v_{dc,i}\right) \tag{16b}$$

where $v_{dc,i}$ is an adjustable non-zero constant that can be predefined. The power series of DC nodal voltage $V_{dc,i}(\alpha)$ is derived as:

$$V_{dc,i}(\alpha)=\sum_{q=0}^{\infty}u_{dc,iq}\alpha^{q} \tag{17}$$

where $u_{dc,iq}$ is the coefficient of the q^{th} term in the power series.

In (16a), at the initial state $\alpha=0$, an initial value of $V_{dc,i}(0)$ equals $v_{dc,i}$. At the target state $\alpha=1$, (16) recovers (11) while the nodal DC voltage solution can be retrieved by $V_{dc,i}(1)$. In (16b), $V_{dc,i}(0)=v_{dc,i}$ and $V_{dc,i}(1)=V_{spdc,i}$ are always satisfied for DC bus i under V_{dc}-control. Therefore, conditions 1 and 2 are met.

By substituting specific control parameters of VSC station in practical cases, it is evident that the model (16) can satisfy condition 3: if $K_i\neq 0$, (16a) represents the droop buses. By letting $K_i=0$, (16a) becomes the representation of constant-P_{dc} buses. By adjusting the value of K_i, the proposed DC FFHE model can easily switch between constant-P_{dc} and droop buses. Moreover, any modification of parameters related to K_i, $V_{ref,i}$, and $V_{spdc,i}$ cannot change the structure of the proposed model, ensuring that its analyzability remains unchanged.

C. Solution Scheme for AC/DC FFHE Model

1) Recursive Solution Processes for Power Series Coefficients

In order to obtain the PF solution by (15) and (17), the coefficients u_{iq} and $u_{dc,iq}$ in the power series need to be determined. Here, we provide the example calculation procedure for these coefficients of *PQ*, constant-P_{dc}, and droop buses.

To bootstrap the recursive solution process for power series coefficients, initial values v_i and $v_{dc,i}$ are needed, which represent the 0^{th}-order coefficients of $\tilde{V}_i(\alpha)$ and $V_{dc,i}(\alpha)$ at the state of $\alpha=\alpha_0=0$, yielding:

$$u_{i0}=\tilde{V}_i(0)=v_i\neq 0 \tag{18a}$$

$$u_{dc,i0}=V_{dc,i}(0)=v_{dc,i}\neq 0 \tag{18b}$$

Such initial values are defined as the "germ solution" [15], leading the voltage power series to the convergence of an operable HV solution is called the "white germ" [16]. In the HE method, $\alpha=0$ represents the zero power injection and zero shunt current injection state, where $1+\mathrm{j}0$ and 1 are the straightforward white germ solutions. Obviously, by setting $v_i=1+\mathrm{j}0$ and $v_{dc,i}=1$, these values are also the white germ for AC/DC FFHE model. Such germ solution exactly matches the "flat start" condition in iterative PF calculation methods, thus serving as the flat start for FFHE method. By adjusting the values assigning to v_i and $v_{dc,i}$, AC/DC FFHE model possesses the flexibility of germ solution selection in addition to using the flat start, which is the key advantage over the HE method. It should be pointed out that, AC/DC FFHE model is not globally convergent but locally convergent to the HV solution, meaning that the assignment of v_i and $v_{dc,i}$ is not arbitrary. Actually, the PF solutions that lie on the same HV branch as the final PF solution, as well as the solutions near the final PF solution, are collectively regarded as white germ solutions for FFHE. Moreover, when using white germ solutions closer to the final PF solution, FFHE requires fewer series expansion terms to achieve convergence.

By substituting the AC voltage series (15) into (13), we can obtain:

$$\sum_{q=0}^{\infty}u_{iq}^{*}\alpha^{q}\sum_{k=1}^{N}Y_{ik}\sum_{q=0}^{\infty}u_{kq}\alpha^{q}=v_i^{*}\sum_{k=1}^{N}Y_{ik}v_k+\alpha\left(\tilde{S}_i^{*}-v_i^{*}\sum_{k=1}^{N}Y_{ik}v_k\right) \tag{19}$$

By equating the coefficients of α^1, α^2, …, α^q on both sides of (19), the following recurrence relationship is derived:

$$\sum_{m=0}^{1} u_{im}^{*} \sum_{k=1}^{N} Y_{ik} u_{k(1-m)} = \tilde{S}_i^{*} - v_i^{*} \sum_{k=1}^{N} Y_{ik} v_k \quad q=1 \tag{20a}$$

$$\sum_{m=0}^{q} u_{im}^{*} \sum_{k=1}^{N} Y_{ik} u_{k(q-m)} = 0 \quad q \geq 2 \tag{20b}$$

If *PV* buses are included, similar equations can be obtained by substituting (15) into (14), which should be incorporated into the relationship above. Then, by moving the unknown and known variables of (20) to the LHS and RHS, a solvable linear function is given as:

$$\boldsymbol{A}_{ac} \boldsymbol{X}_{ac}[q] = \boldsymbol{B}_{ac} \tag{21}$$

where $\boldsymbol{A}_{ac}$ is a coefficient matrix, which is composed of Y_{ik}, $\tilde{S}_i^{*}$, v_i, and v_i^{*}; $\boldsymbol{X}_{ac}[q]$ is an unknown vector contains u_{iq} and u_{iq}^{*}; and $\boldsymbol{B}_{ac}$ is the known vector associated with u_{im} and u_{im}^{*} for $m<q$, which also involves Y_{ik}, $\tilde{S}_i^{*}$, v_i, and v_i^{*}.

To provide the construction and detail elements of $\boldsymbol{X}_{ac}[q]$, $\boldsymbol{A}_{ac}$, and $\boldsymbol{B}_{ac}$, complex variables are represented by their real and imaginary parts as: $Y_{ik}=G_{ik}+\mathrm{j}B_{ik}$, $u_{iq}=u_{iq}^{\mathrm{Re}}+\mathrm{j}u_{iq}^{\mathrm{Im}}$, $v_i=v_i^{\mathrm{Re}}+\mathrm{j}v_i^{\mathrm{Im}}$. Define subscripts $\mathcal{S}$, $\mathcal{L}\in\mathcal{B}_{PQ}$, and $\mathcal{F}\in\mathcal{B}_{PV}$, which denote the AC slack bus, AC *PQ* bus, and AC *PV* bus, respectively. $\mathcal{B}_{PQ}$ and $\mathcal{B}_{PV}$ are the sets of AC *PQ* buses and AC *PV* buses, respectively. Then, $\boldsymbol{A}_{ac}$, $\boldsymbol{X}_{ac}[q]$, and $\boldsymbol{B}_{ac}$ can be expressed as:

$$\boldsymbol{A}_{ac} = \begin{bmatrix} 1 & 0 & 0 & 0 & 0 & 0 \\ 0 & 1 & 0 & 0 & 0 & 0 \\ C_{\mathcal{LS}} & D_{\mathcal{LS}} & C_{\mathcal{LL}} & D_{\mathcal{LL}} & C_{\mathcal{LF}} & D_{\mathcal{LF}} \\ -D_{\mathcal{LS}} & C_{\mathcal{LS}} & E_{\mathcal{LL}} & J_{\mathcal{LL}} & -D_{\mathcal{LF}} & C_{\mathcal{LF}} \\ C_{\mathcal{FS}} & D_{\mathcal{FS}} & C_{\mathcal{FL}} & D_{\mathcal{FL}} & C_{\mathcal{FF}} & D_{\mathcal{FF}} \\ 0 & 0 & 0 & 0 & v_{\mathcal{F}}^{\mathrm{Re}} & v_{\mathcal{F}}^{\mathrm{Im}} \end{bmatrix} \tag{22a}$$

$$\boldsymbol{X}_{ac}[q] = [\, u_{\mathcal{S}q}^{\mathrm{Re}} \quad u_{\mathcal{S}q}^{\mathrm{Im}} \quad u_{\mathcal{L}q}^{\mathrm{Re}} \quad u_{\mathcal{L}q}^{\mathrm{Im}} \quad u_{\mathcal{F}q}^{\mathrm{Re}} \quad u_{\mathcal{F}q}^{\mathrm{Im}} \,] \tag{22b}$$

$$\boldsymbol{B}_{ac} = \begin{bmatrix} \mathrm{Re}\{\Pi_{\mathcal{S}}\} & \mathrm{Im}\{\Pi_{\mathcal{S}}\} & \mathrm{Re}\{\Pi_{\mathcal{L}}\} & \mathrm{Im}\{\Pi_{\mathcal{L}}\} & \Pi_{\mathcal{FP}} & \Pi_{\mathcal{FV}} \end{bmatrix} \tag{22c}$$

where $\mathrm{Im}\{\cdot\}$ represents the imaginary part of a complex phasor.

The elements of coefficient matrix $\boldsymbol{A}_{ac}$ are listed as:

$$C_{ij} = G_{ij} v_i^{\mathrm{Re}} + B_{ij} v_i^{\mathrm{Im}} \quad i \neq j \tag{23}$$

$$D_{ij} = G_{ij} v_i^{\mathrm{Im}} - B_{ij} v_i^{\mathrm{Re}} \quad i \neq j \tag{24}$$

$$C_{ii} = G_{ii} v_i^{\mathrm{Re}} + B_{ii} v_i^{\mathrm{Im}} + \sum_{k=1}^{N} \left(G_{ik} v_k^{\mathrm{Re}} - B_{ik} v_i^{\mathrm{Im}} \right) \tag{25}$$

$$D_{ii} = G_{ii} v_i^{\mathrm{Im}} - B_{ii} v_i^{\mathrm{Re}} + \sum_{k=1}^{N} \left(G_{ik} v_k^{\mathrm{Im}} + B_{ik} v_k^{\mathrm{Re}} \right) \tag{26}$$

$$E_{ii} = -G_{ii} v_i^{\mathrm{Im}} + B_{ii} v_i^{\mathrm{Re}} + \sum_{k=1}^{N} \left(G_{ik} v_k^{\mathrm{Im}} + B_{ik} v_k^{\mathrm{Re}} \right) \tag{27}$$

$$J_{ii} = G_{ii} v_i^{\mathrm{Re}} + B_{ii} v_i^{\mathrm{Im}} + \sum_{k=1}^{N} \left(-G_{ik} v_k^{\mathrm{Re}} + B_{ik} v_k^{\mathrm{Im}} \right) \tag{28}$$

The elements of known vector $\boldsymbol{B}_{ac}$ are listed as (29)-(32), where $\lambda=1$ if $q=1$ and $\lambda=0$ if $q\geq 2$.

$$\Pi_{\mathcal{S}} = \lambda \left(V_{sp,\mathcal{S}} - v_{\mathcal{S}} \right) \tag{29}$$

$$\Pi_{\mathcal{L}} = \lambda \left(\tilde{S}_{\mathcal{L}}^{*} - v_{\mathcal{L}}^{*} \sum_{k=1}^{N} Y_{\mathcal{L}k} v_k \right) - \sum_{k=1}^{N} \sum_{m=1}^{q-1} Y_{\mathcal{L}k} u_{\mathcal{L}m}^{*} u_{k(q-m)} \tag{30}$$

$$\Pi_{\mathcal{FV}} = \frac{\lambda}{2} \left(V_{sp,\mathcal{F}}^{2} - v_{\mathcal{F}} v_{\mathcal{F}}^{*} \right) - \frac{1}{2} \sum_{m=1}^{q-1} u_{\mathcal{F}m} u_{\mathcal{F}(q-m)}^{*} \tag{31}$$

$$\Pi_{\mathcal{FP}} = \frac{\lambda}{2} \left(2P_{\mathcal{F}} - \mathrm{Re}\left\{ v_{\mathcal{F}} \sum_{k=1}^{N} Y_{\mathcal{F}k}^{*} v_k^{*} \right\} \right) - \mathrm{Re}\left\{ \sum_{k=1}^{N} \sum_{m=1}^{q-1} Y_{\mathcal{F}k} u_{\mathcal{F}m}^{*} u_{k(q-m)} \right\} \tag{32}$$

Thus, u_{iq}^{Re} and u_{iq}^{Im} can be successively determined by solving $\boldsymbol{X}_{ac}[q]$ via the following recursive solution process:

$$\tilde{V}_i(0) \xrightarrow{(18a)} \begin{matrix} u_{i0}^{\mathrm{Re}} \\ u_{i0}^{\mathrm{Im}} \end{matrix} \xrightarrow{(21)} \begin{matrix} u_{i1}^{\mathrm{Re}} \\ u_{i1}^{\mathrm{Im}} \end{matrix} \xrightarrow{(21)} \begin{matrix} u_{i2}^{\mathrm{Re}} \\ u_{i2}^{\mathrm{Im}} \end{matrix} \xrightarrow{(21)} \cdots \xrightarrow{(21)} \begin{matrix} u_{il}^{\mathrm{Re}} \\ u_{il}^{\mathrm{Im}} \end{matrix} \tag{33}$$

For the DC FFHE model, supposing $p=1$ for simplicity, (34) is derived by substituting the DC voltage series (17) into (16).

$$\sum_{q=0}^{\infty} u_{dc,iq} \alpha^{q} \left(\sum_{k=1}^{M} G_{ik} \sum_{q=0}^{\infty} u_{dc,kq} \alpha^{q} + K_i \right) = v_{dc,i} \sum_{k=1}^{M} \left(G_{ik} v_{dc,k} + K_i \right) + \alpha \left[K_i V_{ref,i} + P_{ref,i} - v_{dc,i} \sum_{k=1}^{M} \left(G_{ik} v_{dc,k} + K_i \right) \right] \tag{34}$$

Similar to the AC case, the comparison of series coefficients in (34) leads to:

$$\sum_{m=0}^{1} u_{dc,im} \sum_{k=1}^{M} G_{ik} u_{dc,k(1-m)} + K_i u_{dc,i1} = K_i V_{ref,i} + P_{ref,i} - v_{dc,i} \left(\sum_{k=1}^{M} G_{ik} v_{dc,k} + K_i \right) \quad q=1 \tag{35a}$$

$$\sum_{m=0}^{q} u_{dc,im} \sum_{k=1}^{M} G_{ik} u_{dc,k(q-m)} + K_i u_{dc,iq} = 0 \quad q \geq 2 \tag{35b}$$

Then, (35) yields the following linear function:

$$\boldsymbol{A}_{dc} \boldsymbol{X}_{dc}[q] = \boldsymbol{B}_{dc} \tag{36}$$

where $\boldsymbol{X}_{dc}[q]$ is an unknown vector contains $u_{dc,iq}$; $\boldsymbol{A}_{dc}$ is a coefficient matrix, which is composed of G_{ik}, $V_{ref,i}$, $P_{ref,i}$, K_i, and $v_{dc,i}$; and $\boldsymbol{B}_{dc}$ is the known vector associated with $u_{dc,im}$ for $m<q$, which also involves G_{ik}, $V_{ref,i}$, $P_{ref,i}$, K_i, and $v_{dc,i}$. Define subscripts $\mathcal{G}\in\mathcal{B}_{P_{dc},Drp}$ and $\mathcal{H}\in\mathcal{B}_{V_{dc}}$, which denote the DC constant-P_{dc} and droop bus and the constant-V_{dc} bus, respectively. $\mathcal{B}_{P_{dc},Drp}$ and $\mathcal{B}_{V_{dc}}$ are the set of DC constant-P_{dc} and droop buses and the set of constant-V_{dc} buses, respectively.

The constructions of matrix $\boldsymbol{A}_{dc}$, known vector $\boldsymbol{B}_{dc}$, and unknown vector $\boldsymbol{X}_{dc}$ are given as:

$$\boldsymbol{A}_{dc} = \begin{bmatrix} 1 & 0 \\ W_{\mathcal{HG}} & W_{\mathcal{HH}} \end{bmatrix} \tag{37a}$$

$$\boldsymbol{X}_{dc} = \begin{bmatrix} u_{dc,\mathcal{G}q} \\ u_{dc,\mathcal{H}q} \end{bmatrix} \tag{37b}$$

$$\boldsymbol{B}_{dc} = \begin{bmatrix} \Pi_{\mathcal{G}} \\ \Pi_{\mathcal{H}} \end{bmatrix} \tag{37c}$$

The elements of coefficient matrix $\boldsymbol{A}_{dc}$ are listed as:

$$W_{ij} = G_{ij} v_{dc,i} \quad i \neq j \tag{38}$$

$$W_{ii}=G_{ii}v_{dc,i}+\sum_{k=1}^{N}G_{ik}v_{dc,k}+K_i \tag{39}$$

The elements of known vector $\boldsymbol{B}_{ac}$ are as listed as (40) and (41), where $\lambda=1$ if $q=1$ and $\lambda=0$ if $q\geq 2$.

$$\Pi_{\mathcal{G}}=\lambda\left(V_{spdc,\mathcal{G}}-v_{\mathcal{G}}\right) \tag{40}$$

$$\Pi_{\mathcal{H}}=\lambda\left[K_iV_{ref,i}+P_{ref,i}-v_{dc,\mathcal{H}}\left(\sum_{k=1}^{M}G_{\mathcal{H}k}v_{dc,k}+K_i\right)\right]-\sum_{k=1}^{M}\sum_{m=1}^{q-1}u_{dc,\mathcal{H}m}G_{\mathcal{H}k}u_{dc,k(q-m)} \tag{41}$$

Then, $u_{dc,iq}$ can be sequentially obtained according to the following recursive solution process:

$$V_{dc,i}(0)\overset{(18b)}{\rightarrow}u_{dc,i0}\overset{(36)}{\rightarrow}u_{dc,i1}\overset{(36)}{\rightarrow}u_{dc,i2}\overset{(36)}{\rightarrow}\ldots\overset{(36)}{\rightarrow}u_{dc,il} \tag{42}$$

2) Computation of Power Series by Padé Approximant

According to [16], [29], Padé approximant, an ideal rational approximant, is used in the HE and FFHE to converge the numerical solutions of $\tilde{V}_i(\alpha)$ and $V_{dc,i}(\alpha)$ by the function (43) with the obtained u_{iq} and $u_{dc,iq}$ in Section III-C-1).

$$\tilde{V}_i(\alpha)\approx\left[L/M\right]_i(\alpha)=\frac{a_{i0}+a_{i1}\alpha+a_{i2}\alpha^2+\ldots+a_{iL}\alpha^L}{b_{i0}+b_{i1}\alpha+b_{i2}\alpha^2+\ldots+b_{iL}\alpha^M} \tag{43}$$

where $\left[L/M\right]_i(\alpha)$ is the fractional approximation form of the power series truncation; and a_{iq} and b_{iq} can be determined according to [34]. Then, the solution of the original PF equation is provided by $\tilde{V}_i(1)\approx\left[L/M\right]_i(1)$.

The acceleration of the Padé approximant can be achieved by evaluating the ratio of matrix determinants without the need to explicitly calculate a_{iq} and b_{iq}, as described in [29]. Employing such accelerated Padé approximant in our proposed method results in significantly improved computational efficiency.

In brief, FFHE can be implemented through the following procedure.

Step 1: set the initial values of u_{i0} and $u_{dc,i0}$ by selecting v_i and $v_{dc,i}$. Set $q=1$.

Step 2: construct the linear functions (21) and (36) and determine the coefficients of matrices $\boldsymbol{A}_{ac}$ and $\boldsymbol{A}_{dc}$ and vectors $\boldsymbol{B}_{ac}$ and $\boldsymbol{B}_{dc}$.

Step 3: calculate the q^{th} unknown vectors $\boldsymbol{X}_{ac}[q]$ and $\boldsymbol{X}_{dc}[q]$ by solving (21) and (36).

Step 4: calculate the numerical PF solutions $\tilde{V}_i$ for all $i\in N$ or $V_{dc,i}$ for all $i\in M$ at $\alpha=1$ by accelerated Padé approximant. Obtain coefficients in power series.

Step 5: check whether the power mismatch meets the predetermined tolerance for AC PQ and AC PV buses $i\in N$ according to (44a) or for DC bus $i\in M$ according to (44b) under constant-P_{dc} and droop control. If yes, stop the computation of FFHE; otherwise, set $q=q+1$ and return to *Step 2*.

$$\varepsilon_{ac}>\max\left\{\max_{i\in\mathcal{B}_{PQ}\cup\mathcal{B}_{PV}}\left|\mathrm{Re}\left\{\tilde{V}_i\sum_{k=1}^{N}Y_{ik}^{*}\tilde{V}_k^{*}\right\}-\tilde{S}_i\right|,\max_{i\in\mathcal{B}_{PQ}}\left|\mathrm{Im}\left\{\tilde{V}_i\sum_{k=1}^{N}Y_{ik}^{*}\tilde{V}_k^{*}-\tilde{S}_i\right\}\right|\right\} \tag{44a}$$

$$\varepsilon_{dc}>\max_{i\in\mathcal{B}_{P_{dc},Drp}}\left\{\left|V_{dc,i}\sum_{k=1}^{M}G_{ik}V_{dc,k}+K_i\left(V_{dc,i}-V_{ref,i}\right)-P_{ref,i}\right|\right\} \tag{44b}$$

where ε_{ac} is the AC tolerated error; and ε_{dc} is the DC tolerated error.

IV. Sequential Calculation Framework for AC/DC FFHE PF Method

Utilizing the AC/DC FFHE model and its solution scheme proposed in Section III, the PF solutions in AC and DC subsystems can be solved separately. However, to develop the AC/DC FFHE PF method, a key challenge is to establish a proper solving sequence and data exchange mechanism under the constraints of the converter equations. Furthermore, the converter control mode switching can impact the computational efficiency and accuracy of the proposed method. Hence, the impact of converter control mode switching on the proposed method needs to be further examined and discussed.

A. Calculation Process and Data Exchange

The flow chart of the calculation process of AC/DC FFHE PF method is shown in Fig. 2. A sequential calculation framework is applied to solve the PF in AC subsystems, DC subsystems, and converter station separately.

Step 1: initialization. Load the system data of AC and DC subsystems. Set the initial values of u_{i0} and $u_{dc,i0}$ by assigning values to v_i and $v_{dc,i}$ in the FFHE model. Set tolerated errors ε_{ac}, ε_{dc}, and $\varepsilon_{ac/dc}$.

Step 2: execution of AC FFHE. Given predetermined converter control modes, the PCC bus is treated as either a PQ bus (P_s and Q_s are known) or a PV bus (P_s and V_s are known) in PF calculation. Combining with all the pure AC buses in the AC system, voltage solution $\tilde{V}_s$ at the PCC bus can be obtained by executing the AC FFHE.

Step 3: converter calculation. With the known and determined parameters of PCC buses, the operational state, including $\tilde{S}_c=P_c+\mathrm{j}Q_c$ and $\tilde{V}_c$ of the PAC buses, is easily obtained according to (1)-(3). Then, the active power losses of VSC can be calculated by (5) and (6).

Step 4: data exchange (AC to DC). Given the active power losses, the active power P_{dc} injected from VSC into PDC buses is determined by (4). Note that, by making P_{ref} equal P_{dc}, the parameters associated with the constant-P_{dc} buses ($K=0$) required for solving (11) become known.

Step 5: execution of DC FFHE. Given the known parameters of P_{ref}, V_{ref}, K for droop buses, V_{dc} for constant-V_{dc} buses, and the latest obtained P_{ref} for constant-P_{dc} buses, the DC FFHE is executed. Solutions include the V_{dc} for constant-P_{dc} and droop buses, and P_{dc} for constant-V_{dc} and droop buses.

Step 6: data exchange (DC to AC). With the newly calculated active power of PDC buses under constant-V_{dc} and droop buses, a new active power injection $P_c^{(new)}$ from VSC to PAC buses is updated by (4).

Step 7: check of termination criterion. A new active power injection at the i^{th} PCC bus $P_{s,i}^{(new)}$ can be updated via the con-

verter calculation (1)-(3) with $P_c^{(new)}$ calculated in *Step 6*, and the calculation will be terminated if (45) is satisfied, where $\mathcal{B}_{PCC}$ is the set of PCC buses, and $P_{s,i}^{(old)}$ is the previous calculated active power injection at PCC bus. Otherwise, a new round of calculation with $P_s^{(new)}$ is started.

$$\varepsilon_{ac/dc} > \max_{i \in \mathcal{B}_{PCC}} \left\{ P_{s,i}^{(new)} - P_{s,i}^{(old)} \right\} \tag{45}$$

Note that, if the termination criterion is not met, the current PF results will be assigned to v_i and $v_{dc,i}$ before returning to *Step 2*. These values will be directly used as the initial state for the next round of AC/DC PF calculation.

In summary, within the proposed sequential calculation framework, the PF of AC and DC subsystems can be calculated independently using the proposed FFHE model, while the AC/DC data interaction is facilitated by converter station calculation and data exchange mechanism. The advantage of this sequential calculation framework lies in its strong scalability to different grid topologies and scales of AC and DC subsystems, as well as various configurations and operation modes of VSC stations. The corresponding modification to any individual part in the sequential calculation framework can be simply and directly implemented without affecting other parts.

B. VSC Control Mode Switching

Due to the output power constraints of the converter and the voltage limitations of the converter bus, the converter control mode is crucial for conducting the AC/DC PF calculation. By evaluating $\tilde{S}_c$ and $\tilde{V}_c$ at the PAC buses, VSC control modes will be switched between Q_s-control and V_s-control [8] if the limits are exceeded. We propose a scheme to implement the VSC control mode switching mechanism for the AC/DC FFHE. An example of switching from Q_s-control to V_s-control is presented as below.

Step 1: suppose the VSC is working under Q_s-control.

Step 2: solve PF by the AC/DC FFHE and save the PF solutions. These solutions will be used in the limit check, as well as utilized as the initial values for the new round of AC/DC FFHE if needed.

Step 3: conduct VSC limit check and determine the PAC buses that hit the $\tilde{V}_c$ limits using the saved PF solutions. Switch to V_s-control mode if the limits are exceeded.

Step 4: assign the current PF solutions to v_i and $v_{dc,i}$ as the default start, and repeat *Step 2* and *Step 3* until all VSC limits are met.

The switching from V_s-control to Q_s-control can be realized using the same mechanism.

It is worth noting that, in either the sequential calculation framework described in Section IV-A to achieve overall AC/DC PF convergence or after a VSC control mode switching described in this subsection, multiple recalculations are always necessary. Fortunately, even if the overall termination criterion is not met or the converter control mode needs to be switched, the newly calculated intermediate PF solutions often closely approximate the final solution. Benefiting from the flexibility of initialization (germ solution selection) of the proposed AC/DC FFHE model, these intermediate solutions can be directly utilized for the AC/DC FFHE PF method as the white germ, achieved by assigning current solutions to v_i and $v_{dc,i}$, as shown in Fig. 2. This results in a notable reduction in both the required calculation steps and the number of necessary series expansion terms of the AC/DC FFHE PF method, providing higher computational efficiency compared with the HE method, which can only be initialized from a flat start.

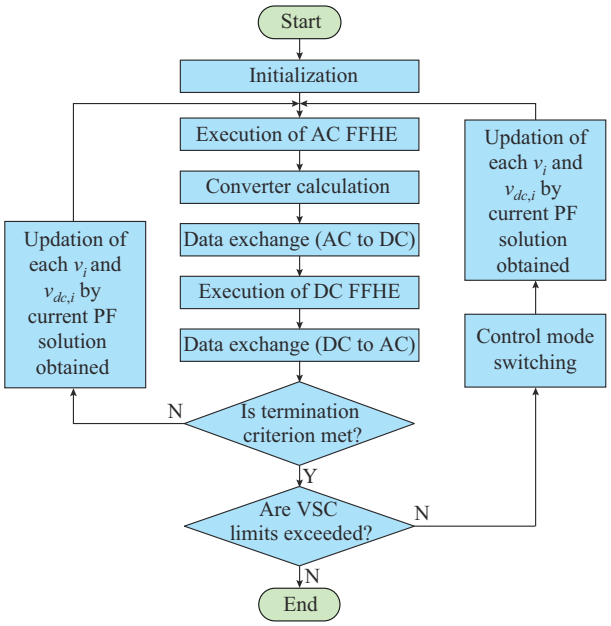

Fig. 2. Flow chart of calculation process of AC/DC FFHE PF method.

V. Numerical Tests

In this section, numerical performance of the proposed AC/DC FFHE PF method will be demonstrated by multiple simulations on two test systems. Test system A comprises a 5-bus AC grid (ACS) interconnected with a 3-bus DC grid (DCS), as shown in Fig. 3. Test system B is modeled after the IEEE RTS-96 system, featuring three AC grids (ACS1, ACS2, and ACS3) and the incorporation of two DC grids (DCS1 and DCS2), as depicted in Fig. 4. The parameters for both test systems A and B are consistent with the values provided in [35], [36]. All the numerical tests are implemented using MATLAB installed on PC with Intel(R) Core(TM) i7-7700HQ CPU @ 2.80 GHz and 16 GB RAM.

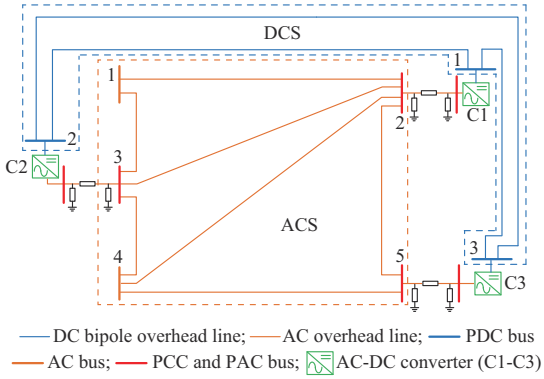

Fig. 3. Test system A.

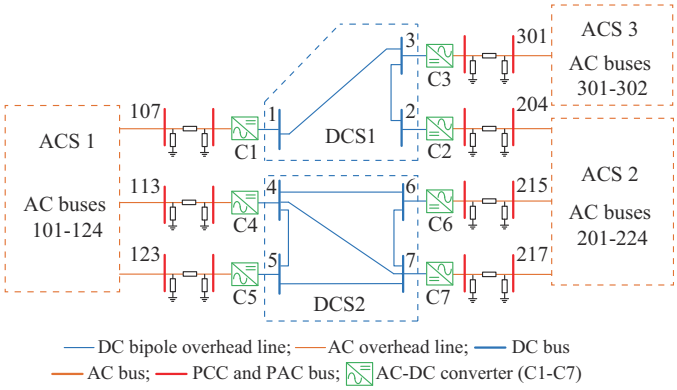

Fig. 4. Test system B.

A. Accuracy Verification

In this subsection, to verify the accuracy of the proposed AC/DC FFHE PF method, both the N-R-based method in [8] and the proposed method are implemented to solve PF in the test system A. AC bus 1 is defined as the slack bus with reference voltage $\tilde{V}_1 = (1.0600 + \mathrm{j}1.0000)$ p. u., and AC bus 2 is a *PV* bus with AC voltage magnitude $\left|\tilde{V}_2\right| = 1.0000$ p. u.. All of the rest AC buses are operating as *PQ* buses. The DC bus 2 is under constant-V_{dc} mode maintaining $V_{dc,1} = 1.0000$ p. u., and all of the rest DC buses are working under constant-P_{dc} mode. The flat start, $v_i = 1 + \mathrm{j}0$, and $v_{dc,i} = 1$ are used as the germ solutions to initialize both methods and the tolerated error is set to be $\varepsilon_{ac} = \varepsilon_{dc} = \varepsilon_{ac/dc} = 10^{-6}$. The results of the N-R-based method are regarded as the reference.

The proposed method converges to the final solutions after 3 overall calculations. Tables II and III present the power series coefficients of AC voltage $\tilde{V}_i(\alpha)$ and DC voltage $V_{dc,i}(\alpha)$ calculated in the 1st AC and DC FFHE process. As shown in Table II, the proposed method needs to calculate power series coefficients of 6 terms of AC voltage to satisfy the termination criterion. Note that, starting from the 4th term, the coefficients are smaller than 1×10^{-6} and approach 0. The proposed method is required to calculate power series coefficients of 5 terms of DC voltage to satisfy the termination criterion, with coefficients smaller than 1×10^{-6} starting from the 4th term.

TABLE II
POWER SERIES COEFFICIENTS OF $\tilde{V}_i(\alpha)$ IN THE 1ST AC FFHE PROCESS

Power series coefficient	$\tilde{V}_1(\alpha)$	$\tilde{V}_2(\alpha)$	$\tilde{V}_3(\alpha)$	$\tilde{V}_4(\alpha)$	$\tilde{V}_5(\alpha)$
u_{i0}	1 + j0	1 + j0	1 + j0	1 + j0	1 + j0
u_{i1}	0.6 + j0	0.0000 – j0.0419	0.0020 – j0.0666	–0.0023 – j0.0732	–0.0083 – j0.0720
u_{i2}	0	–0.0000 + j0.0021	–0.0032 + j0.0025	–0.0030 + j0.0026	–0.0033 + j0.0027
u_{i3}	0	0.0001 – j0.0001	0.0002 – j0.0001	0.0002 – j0.0001	0.0002 – j0.0001
u_{i4}	0	0.0000 + j0.0000	0.0000 + j0.0000	0.0000 + j0.0000	0.0000 + j0.0000
u_{i5}	0	0.0000 + j0.0000	0.0000 + j0.0000	0.0000 + j0.0000	0.0000 + j0.0000

TABLE III
POWER SERIES COEFFICIENTS OF $V_{dc,i}(\alpha)$ IN THE 1ST DC FFHE PROCESS

Power series coefficient	$V_{dc,1}(\alpha)$	$V_{dc,2}(\alpha)$	$V_{dc,3}(\alpha)$
$u_{dc,i0}$	1.0000	1	1.0000
$u_{dc,i1}$	0.0080	0	0.0022
$u_{dc,i2}$	–0.0001	0	–0.0001
$u_{dc,i3}$	0.0000	0	0.0000
$u_{dc,i4}$	0.0000	0	0.0000

By letting $\alpha = 1$ and substituting power series coefficients into (15) and (17), the nodal AC/DC voltage solution listed in Tables IV and V can be obtained via accelerated Padé approximant. The operation conditions of VSC stations are also evaluated according to the final solutions, as presented in Table VI. Based on the results, it can be observed that the calculated PF solutions in test system A using the proposed method are in complete agreement with the results obtained by the N-R-based method. The maximum error is observed in calculated bus power values of the VSC station, yet its relative error remains below 0.1%. This validates the accuracy of the proposed method.

TABLE IV
COMPARISON OF NODAL AC VOLTAGE SOLUTIONS OBTAINED BY PROPOSED AND N-R-BASED METHODS

AC bus No.	Proposed method		N-R-based method	
	Voltage magnitude (p.u.)	Voltage angle (°)	Voltage magnitude (p.u.)	Voltage angle (°)
1	1.0600	0.0000	1.0600	0.0000
2	1.0000	–2.3829	1.0000	–2.3829
3	1.0000	–3.8947	1.0000	–3.8947
4	0.9960	–4.2608	0.9960	–4.2608
5	0.9908	–4.1489	0.9908	–4.1489

TABLE V
COMPARISON OF NODAL DC VOLTAGE SOLUTIONS OBTAINED BY PROPOSED AND N-R-BASED METHODS

DC bus No.	Voltage magnitude of proposed method (p.u.)	Voltage magnitude of N-R-based method (p.u.)
1	1.0079	1.0079
2	1.0000	1.0000
3	0.9978	0.9978

TABLE VI
OPERATION CONDITIONS OF VSC STATIONS IN TEST SYSTEM A

VSC station	PAC bus voltage		PAC bus power (p.u.)	PDC bus power (p.u.)	Power loss (p.u.)
	Magnitude (p.u.)	Angle (°)			
C1	0.8899	–13.0167	–0.5992–j0.3263	0.5863	0.0128
C2	1.0070	–0.6517	0.2078–j0.0065	–0.2190	0.0114
C3	0.9955	1.4421	0.3502–j0.0037	–0.3619	0.0117

B. Efficiency Comparison

In this subsection, we will demonstrate the computational efficiency of the proposed method compared with existing methods, including the N-R-based and HE methods. It is important to note that, due to variations in programming techniques, simulation platforms, computer performance, and other factors, the computational time presented in this subsection may not necessarily be universally applicable. Nevertheless, the comparative analysis conducted uniformly on the MATLAB 2023(a) platform on the same PC for different methods remains a valuable reference.

Then, we focus on the comparison between HE-based and proposed methods. The two methods are employed to solve the PF of test system B from a flat start, considering the maximum tolerated error $\{\varepsilon | \varepsilon_{ac}, \varepsilon_{dc}, \varepsilon_{ac/dc}\}$ ranging from 1×10^{-3} to 1×10^{-9}. Figures 5 and 6 present the required number of series terms and the corresponding runtime to complete the 1st-round AC/DC PF calculation in test systems A and B, respectively. As observed, the accelerated Padé approximant employed in handling the summation of power series significantly reduces the required number of series terms for the proposed method compared with that of the HE method. This consequently leads to a substantial reduction in runtime.

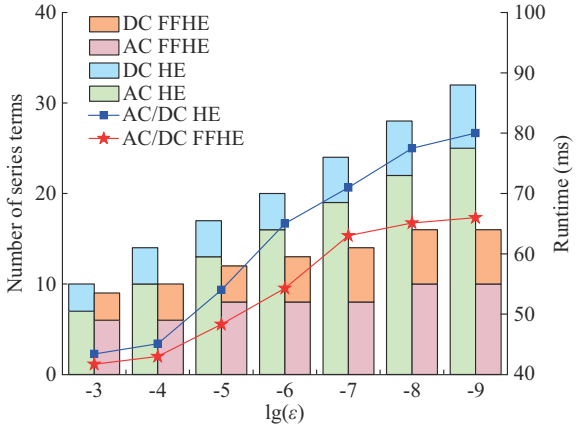

Fig. 5. Required number of series terms and runtime to complete the 1st-round AC/DC PF calculation in test system A.

Moreover, after completing a full round of overall AC/DC PF calculation, if the AC/DC PF has not converged in the converter station calculation, both methods necessitate an update of the PCC bus parameters at the converter station and proceed to the next round of overall calculation. It should be noted that even if the termination criterion is not met, the current PF solution is usually very close to the final solution. Recalculating from a flat start without utilizing this latest PF solution would result in significant redundant calculations and reduce the efficiency of the proposed method. The sequential calculation framework depicted in Fig. 2 enables the latest PF solution to be assigned to v_i and $v_{dc,i}$, which are used directly for the subsequent FFHE recursive solution processes. In contrast, the HE method requires a recalculation starting from the flat start. This results in a significantly reduced overall runtime for the proposed method compared with the HE method, with the runtime approaching or even falling below that of the N-R-based method, as shown in Fig. 7.

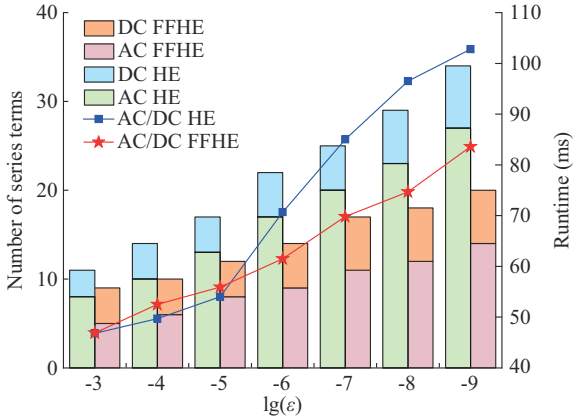

Fig. 6. Required number of series terms and runtime to complete the 1st-round AC/DC PF calculation in test system B.

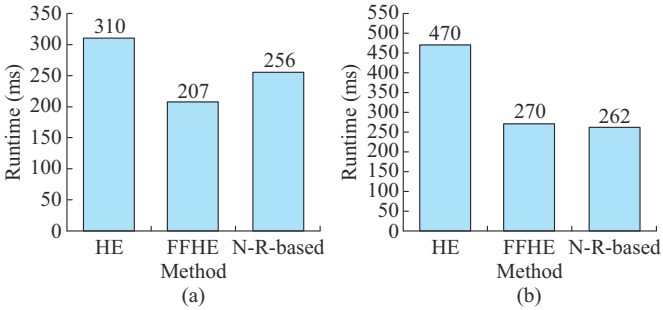

Fig. 7. Overall runtime comparison. (a) Overall runtime for test system A. (b) Overall runtime for test system B.

C. Impact of Different Types of Initializations

In the AC/DC FFHE solving process, there are three scenarios that require initialization. In scenario 1, the proposed method necessitates initial value settings at the outset. In scenario 2, unless the overall AC/DC PF convergence is achieved, initializations are needed to start new AC and DC FFHE solving processes with the updated converter station parameters. In scenario 3, when the converter reaches the power limit constraint, leading to a control mode switching, FFHE initializations are also required. Here, we define two types of initializations: ① using $v_i = 1 + \mathrm{j}0$ and $v_{dc,i} = 1$ as a flat start; and ② using the known or the last obtained PF solution as the default start. In our test cases, we consistently employ a flat start as the overall initial value for scenario 1. By changing the initial values for scenarios 2 and 3, the impact of different types of initializations on the proposed

method can be analyzed.

For DC FFHE solving process, as the DC PF solution is generally very close to 1 p.u., the choice of two types of initializations has a minimal impact on its required calculational steps and runtime. Therefore, our focus is on the AC FFHE solving process. For bus 4 and bus 5 in the ACS of test system A, the initial values v_4 and v_5 for these two buses are selected to vary within the following range: the real part v_4^{Re} ranges from 0.94 p.u. to 1.04 p.u. and the imaginary part v_4^{Im} ranges from −0.0850 p.u. to 0.0850 p.u. for v_4, while the real part v_5^{Re} ranges from 0.92 p.u. to 1.02 p.u. and the imaginary part v_5^{Im} ranges from −0.0976 p.u. to 0.0976 p.u. for v_5. The number of series terms required for the proposed method meets a tolerance of $\varepsilon_{ac}=10^{-6}$, which can reflect its convergence performance under different types of initializations. As shown in Figs. 8 and 9, the structure of the convergence area organized by the required number of series terms varies when different initial values for buses are selected. For instance, during the AC FFHE calculation for the ACS of test system A, within the same range of variation, the proposed method exhibits greater sensitivity to the initial value of bus 4 compared with that of bus 5, leading to a larger number of required series terms. As observed from Fig. 8, it is evident that the AC FFHE fails to achieve the global convergence. As the solution deviates from the true solution (0.9804 – j0.0850)p.u., the required number of series terms significantly increases and exceeds 50. Although it is possible that the AC FFHE process might converge with more series terms, it still significantly reduces the efficiency of the AC FFHE process, making its performance unsatisfactory.

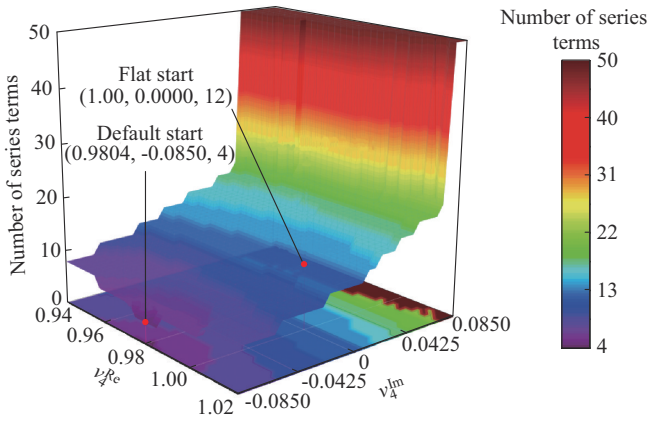

Fig. 8. Required number of series terms with variation of initialization for bus 4 in test system A.

Meanwhile, it can be observed that the AC FFHE method requires 12 series terms when starting the calculation from a flat start, while starting the calculation from or close to the default start only requires 4 series terms. It is worth noting that, in both scenarios 2 and 3, although the AC/DC PF does not achieve overall convergence at the 1st round of AC/DC FFHE calculation, the latest PF solution obtained is very close to the actual solution. The unique structure of the AC FFHE method takes advantage of these solutions as a default start condition. As shown in Table VII, utilizing such default start condition significantly reduces the number of series terms required for subsequent AC FFHE calculation, thereby decreasing the runtime. For example, under the tolerance of 1×10^{-6}, when a default start is used, convergence can be achieved with only 4 series terms in each subsequent calculation, starting from the 2nd round of AC FFHE calculation. In contrast, AC FFHE calculation with a flat start results in a consistent number of required series terms for each subsequent calculation.

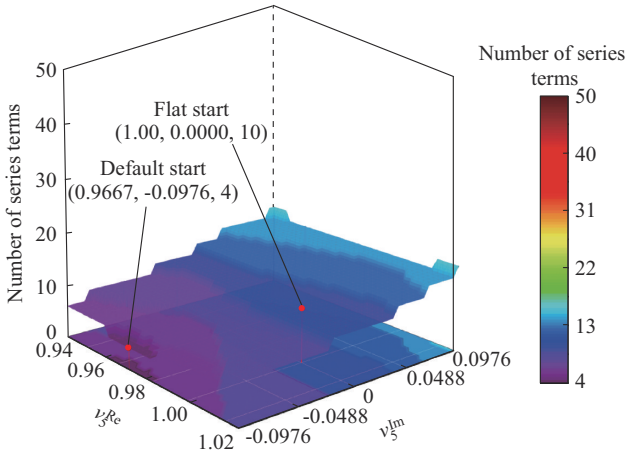

Fig. 9. Required number of series terms with variation of initialization for bus 5 in test system A.

TABLE VII
IMPACT OF DIFFERENT TYPES OF INITIALIZATIONS WITHOUT CONTROL MODE SWITCHING

lg(ε)	Flat start		Default start	
	Number of series terms	Runtime (ms)	Number of series terms	Runtime (ms)
–4	[6, 6]	112	[6, 4]	97
–6	[8, 8, 8]	285	[8, 4, 4]	159
–8	[10, 10, 10, 10]	397	[10, 4, 4, 4]	212

Note: [6, 6] represents that the numbers of series terms in the 1st and 2nd rounds are 6 and 6, respectively; and the meaning of other data can be inferred similarly.

Similar results are obtained when testing the control mode switching of test systems A and B. We adjust the power limit of VSCs at PCC bus 2 in test system A and the power limit of VSCs at PCC buses 203 and 207 in test system B. Due to the exceedance of the limits, the control mode of these VSCs has to be switched from V_s-control to Q_s-control. With regard to the required runtime, it can be observed from Table VIII that the implementation of default start can significantly reduce the total runtime. The reduction of test system A is 27.6%, while that of test system B is 38.1%.

TABLE VIII
IMPACT OF DIFFERENT TYPES OF INITIALIZATIONS WITH CONTROL MODE SWITCHING

Test system	Runtime (ms)		Reduced runtime (%)
	Flat start	Default start	
Test system A	380	275	27.60
Test system B	486	301	38.10

VI. Conclusion

This paper presents a novel PF calculation method based on the FFHE for VSC-based AC/DC hybrid systems. The proposed method consists of an AC/DC FFHE model and a sequential calculation framework. The proposed AC/DC FFHE model exhibits remarkable flexibility in its structure, allowing for systematic adaption to various bus types under different VSC control modes. A sequential calculation framework is designed combining solution scheme for the AC/DC FFHE model with AC/DC data exchange and control mode switching mechanisms. The initialization flexibility of AC/DC FFHE PF method facilitates the reduction of runtime and required number of series terms, resulting in superior computational efficiency, especially when recalculations are required to achieve overall AC/DC PF convergence or after VSC control mode switching. Multiple numerical tests demonstrate that the proposed method retains the advantages of the HE method in terms of accurate and reliable convergence to feasible solutions, while also exhibiting higher computational efficiency than that of the existing methods.

In future, two potential prospects could be focused on. First, to further improve the computational efficiency of the proposed method, the research on code optimization and the integration of parallel computing techniques is required. Second, the utilization of FFHE to pinpoint PF limit solutions (static voltage stability limits) in AC/DC hybrid systems deserves further investigation.

References

[1] V. Akhmatov, M. Callavik, C. M. Franck *et al*., "Technical guidelines and prestandardization work for first HVDC grids," *IEEE Transactions on Power Delivery*, vol. 29, no. 1, pp. 327-335, Feb. 2014.

[2] Y. Wang, F. Qiu, G. Liu *et al*., "Adaptive reference power based voltage droop control for VSC-MTDC systems," *Journal of Modern Power Systems and Clean Energy*, vol. 11, no. 1, pp. 381-388, Jan. 2023.

[3] R. Chen, D. Ke, Y. Sun *et al*., "Hierarchical frequency-dependent chance constrained unit commitment for bulk AC/DC hybrid power systems with wind power generation," *Journal of Modern Power Systems and Clean Energy*, vol. 11, no. 4, pp. 1053-1064, Jul. 2023.

[4] Acha, B. Kazemtabrizi, and L. M. Castro, "A new VSC-HVDC model for power flows using the Newton-Raphson method," *IEEE Transactions on Power Systems*, vol. 28, no. 3, pp. 2602-2612, Aug. 2013.

[5] R. Chai, B. Zhang, J. Dou *et al*., "Unified power flow algorithm based on the NR method for hybrid AC/DC grids incorporating VSCs," *IEEE Transactions on Power Systems*, vol. 31, no. 6, pp. 4310-4318, Nov. 2016.

[6] Z. S. Molaee, E. Rokrok, and M. Doostizadeh, "A unified power flow approach using VSC-efficiency for AC-DC distribution systems operating at grid connected and islanded modes," *International Journal of Electrical Power & Energy Systems*, vol. 130, p. 106906, Sept. 2021.

[7] S. Wang, X. Jiang, Q. Zhao *et al*., "Unified load flow calculation for flexible interconnected AC-MTDC distribution system considering control strategy switching with high penetration of DGs," *International Journal of Electrical Power and Energy Systems*, vol. 131, p. 107130, Oct. 2021.

[8] J. Beerten, S. Cole, and R. Belmans, "Generalized steady-state VSC MTDC model for sequential AC/DC power flow algorithms," *IEEE Transactions on Power Systems*, vol. 27, no. 2, pp. 821-829, May 2012.

[9] W. Wang and M. Barnes, "Power flow algorithms for multi-terminal VSC-HVDC with droop control," *IEEE Transactions on Power Systems*, vol. 29, no. 4, pp. 1721-1730, Jul. 2014.

[10] Y. Zhang, X. Meng, A. Malik *et al*., "The use of analytical converter loss formula to eliminate DC slack/droop bus iteration in sequential AC-DC power flow algorithm," *International Journal of Electrical Power & Energy Systems*, vol. 137, p. 107596, May 2022.

[11] P. Tian, Y. Jin, G. Zhang *et al*., "An implicit Z-bus based sequential power flow algorithm for VSC AC/DC systems," *International Journal of Electrical Power and Energy Systems*, vol. 155, p. 109648, Jan. 2024.

[12] H. Susanto and N. Karjanto, "Newton's method's basins of attraction revisited," *Applied Mathematics and Computation*, vol. 215, no. 3, pp. 1084-1090, Oct. 2009.

[13] S. Amat, I. K. Argyros, S. Busquier *et al*., "Newton-type methods on Riemannian manifolds under Kantorovich-type conditions," *Applied Mathematics and Computation*, vol. 227, pp. 762-787, Jan. 2014.

[14] K. Dvijotham, E. Mallada, and J. W. Simpson-Porco, "High-voltage solution in radial power networks: existence, properties, and equivalent algorithms," *IEEE Control Systems Letters*, vol. 1, no. 2, pp. 322-327, Oct. 2017.

[15] A. Trias, "The holomorphic embedding load flow method," in *Proceedings of 2012 IEEE PES General Meeting*, San Diego, USA, Jul. 2012, pp. 1-5.

[16] A. Trias and J. L. Marin, "The holomorphic embedding load flow method for DC power systems and nonlinear DC circuits," *IEEE Transactions on Circuits and Systems I*: *Regular Papers*, vol. 63, no. 2, pp. 322-333, Feb. 2016.

[17] S. Rao, Y. Feng, D. J. Tylavsky *et al*., "The holomorphic embedding method applied to the power-flow problem," *IEEE Transactions on Power Systems*, vol. 31, no. 5, pp. 3816-3828, Sept. 2016.

[18] S. D. Rao and D. J. Tylavsky, "Theoretical convergence guarantees versus numerical convergence behavior of the holomorphically embedded power flow method," *International Journal of Electrical Power & Energy Systems*, vol. 95, pp. 166-176, Feb. 2018.

[19] M. Basiri-Kejani and E. Gholipour, "Holomorphic embedding load-flow modeling of thyristor-based FACTS controllers," *IEEE Transactions on Power Systems*, vol. 32, no. 6, pp. 4871-4879, Nov. 2017.

[20] P. Singh and N. Senroy, "Steady-state model of VSC based FACTS devices using flexible holomorphic embedding: (SSSC and IPFC)," *International Journal of Electrical Power & Energy Systems*, vol. 133, p. 107256, Dec. 2021.

[21] C. Liu, B. Wang, F. Hu *et al*., "Online voltage stability assessment for load areas based on the holomorphic embedding method," *IEEE Transactions on Power Systems*, vol. 33, no. 4, pp. 3720-3734, Jul. 2018.

[22] Y. Sun, T. Ding, O. Han *et al*., "Static voltage stability analysis based on multi-dimensional holomorphic embedding method," *IEEE Transactions on Power Systems*, vol. 38, no. 4, pp. 3748-3759, Jul. 2023.

[23] Q. Lai, C. Liu, and K. Sun, "Vulnerability assessment for voltage stability based on solvability regions of decoupled power flow equations," *Applied Energy*, vol. 304, p. 117738, Dec. 2021.

[24] Y. Huang, X. Ai, J. Fang *et al*., "Holomorphic embedding approach for VSC-based AC/DC power flow," *IET Generation*, *Transmission & Distribution*, vol. 14, no. 25, pp. 6239-6249, Dec. 2020.

[25] Y. Zhao, C. Li, T. Ding *et al*., "Holomorphic embedding power flow for AC/DC hybrid power systems using Bauer's ETA algorithm," *IEEE Transactions on Power Systems*, vol. 36, no. 4, pp. 3595-3606, Jul. 2021.

[26] U. Sur, A. Biswas, J. N. Bera *et al*., "A modified holomorphic embedding method based hybrid AC-DC microgrid load flow," *Electric Power Systems Research*, vol. 182, p. 106267, May 2020.

[27] M. Y. Morgan, M. F. Shaaban, H. F. Sindi *et al*., "A holomorphic embedding power flow algorithm for islanded hybrid AC/DC microgrids," *IEEE Transactions on Smart Grid*, vol. 13, no. 3, pp. 1813-1825, May 2022.

[28] Y. Huang, X. Ai, J. Fang *et al*., "Holomorphic embedding power flow modeling of autonomous AC/DC hybrid microgrids," *International Journal of Electrical Power & Energy Systems*, vol. 145, p. 108549, Feb. 2023.

[29] H. D. Chiang, T. Wang, and H. Sheng, "A novel fast and flexible holomorphic embedding power flow method," *IEEE Transactions on Power Systems*, vol. 33, no. 3, pp. 2551-2562, May 2018.

[30] T. Wang and H. D. Chiang, "On the holomorphic and conjugate properties for holomorphic embedding methods for solving power flow equations," *IEEE Transactions on Power Systems*, vol. 35, no. 4, pp. 2506-2515, Jul. 2020.

[31] T. Wang and H. D. Chiang, "Theoretical study of non-iterative holomorphic embedding methods for solving nonlinear power flow equations: algebraic property," *IEEE Transactions on Power Systems*, vol. 36, no. 4, pp. 2934-2945, Jul. 2021.

[32] H. Stahl, "On the convergence of generalized Padé approximants," *Constructive Approximation*, vol. 5, no. 1, pp. 221-240, Jan. 1989.

[33] H. Stahl, "The convergence of Padé approximants to functions with branch points," *Journal of Approximation Theory*, vol. 91, no. 2, pp. 139-204, Mar. 1997.

[34] G. A. Baker and P. Graves-Morris, *Padé Approximants*. Cambridge: Cambridge University Press, 1996.
[35] J. Beerten, D. van Hertem, and R. Belmans, "VSC MTDC systems with a distributed DC voltage control – a power flow approach," in *Proceedings of 2011 IEEE Trondheim PowerTech*, Trondheim, Norway, Jun. 2011, pp. 1-6.
[36] J. Beerten. (2021, Feb.). MatACDC. [Online]. Available: http://www.esat.kuleuven.be/electa/teaching/matacdc/

Peichuan Tian received the B.S. degree in electrical engineering and its automation from Shanghai Jiao Tong University, Shanghai, China, in 2017. He received the M.S. degree in electrical and computer engineering from The Ohio State University, Columbus, USA, in 2018. He is now working toward the Ph.D. degree in electrical engineering at Shanghai Jiao Tong University. His main research interests include power flow and system stability analysis in AC/DC hybrid grid.

Yexuan Jin received the B.S. degree in electrical engineering and its automation from Chongqing University, Chongqing, China, in 2017. She received the M.S. degree in electrical engineering from Shanghai Jiao Tong University, Shanghai, China, in 2021. She is now working at State Grid Hangzhou Power Supply Company, Hangzhou, China. Her main research interests include power system operation and dispatching.

Ning Xie received the Ph.D. degree in electrical engineering awarded by Politecnico di Torino, Turin, Italy, in 2011. She joined the Electrical Engineering Department of Shanghai Jiao Tong University, Shanghai, China, in 1998, where she is currently an Associate Professor. Her research interests include power system analysis, operation and planning, electricity market, and smart grid.

Chengmin Wang received the Ph.D. degree in electrical engineering from Harbin Institute of Technology, Harbin, China, in 2002. Since 2005, he has been a Professor with the School of Electronic Information and Electrical Engineering, Shanghai Jiao Tong University, Shanghai, China. His research interests include optimal operation of power system, power system programming, electricity market, and smart grid.

Chunyi Huang received the B.S. and Ph.D. degrees in electrical engineering from North China Electric Power University, Beijing, China, in 2015, and Shanghai Jiao Tong University, Shanghai, China, in 2021. She is currently an Assistant Researcher in Shanghai Jiao Tong University. Her research interests include flexibility optimization of distribution systems and retail electricity market mechanism integrated with massive distributed energy resources.